Design of a plasmonic back reflector using Ag nanoparticles with a mirror support for an a-Si:H solar cell

Cite as: AIP Advances **7**, 075004 (2017); https://doi.org/10.1063/1.4993743
Submitted: 19 April 2017 • Accepted: 29 June 2017 • Published Online: 11 July 2017

Chanse D. Hungerford and Philippe M. Fauchet

Design of a plasmonic back reflector using Ag nanoparticles with a mirror support for an a-Si:H solar cell

Chanse D. Hungerford[1,2,a] and Philippe M. Fauchet[2]
[1]*The Institute of Optics, University of Rochester, Rochester, New York 14627, United States*
[2]*Department of Electrical Engineering and Computer Science, Vanderbilt University, Nashville, Tennessee 37240, United States*

(Received 19 April 2017; accepted 29 June 2017; published online 11 July 2017)

Plasmonic nanoparticles have unique optical properties and these properties are affected by any surrounding structures, or lack thereof. Nanoparticles are often added to a device without fully assessing the effect that each interface will have on the nanoparticle's response. In this work, we simulate and fabricate devices utilizing hemispherical nanoparticles integrated into the back reflector of an amorphous silicon solar cell. 3D finite difference time domain simulations were used to calculate the optical absorption of a 300nm amorphous silicon layer as a function of the size of the nanoparticles, the distance between the nanoparticles and the active layer, and the distance between the nanoparticles and the mirror. Two transparent conducting oxides, aluminum doped zinc oxide and indium tin oxide, are investigated to determine the importance of the material properties between the nanoparticles and mirror. Silver hemispherical nanoparticles with a diameter of 150nm placed directly on the a-Si:H and a 60nm aluminum doped zinc oxide layer between the nanoparticles and the mirror lead to a maximum absorption increase of 7.2% in the 500nm to 800nm wavelength range. Experimental devices confirmed the trends predicted by theory but did not achieve enhancement, likely due to fabrication challenges. Fabricating a solar cell with the simulated design requires a high quality transparent conductive oxide and high control over the nanoparticle size distribution. [http://dx.doi.org/10.1063/1.4993743]

INTRODUCTION

The current solar cell market consists mostly of relatively thick mono- or multi-crystalline, silicon solar cells. These technologies require a large amount of high purity silicon, making the cost dependent on the price of silicon feedstock and silicon wafer processing.[1] One way to avoid these substantial costs is to use thin-film solar cells. One such technology is thin-film hydrogenated amorphous silicon (a-Si:H). While a-Si:H exhibits useful optical properties for solar energy applications, the electrical properties of the material place limitations on device performance and design.[2] Due to short carrier lifetimes, a-Si:H solar cells should be relatively thin. Another issue with a-Si:H solar cells is light induced degradation, known as the Staebler-Wronski effect, and this degradation is generally addressed by further reducing the a-Si:H thickness.[3] Reducing the thickness of the cell leads to a decrease in light absorption. One way to avoid these losses is to employ a light trapping structure, increasing the optical path length of light within the cell.[4] Light trapping for thin film solar is commonly done by using a textured transparent conducting oxide (TCO) as the substrate/superstrate for the solar cell deposition.[5] This method involves a trade-off between optical and electrical performance. High-aspect ratio textures are required for good light trapping,[6]

[a]Corresponding Author: chanse.hungerford@rochester.edu

but can lead to significant defect formation during film growth and negatively impact electrical performance.[7–9] A promising alternative to these high-aspect ratio structures is nanostructures for light trapping. Theory shows that nanostructure may allow for the fabrication for ultra-thin solar cells that can surpass the light trapping limit associated with bulk films.[10] Early work done by Stuart and Hall[11,12] has shown that metallic nanoparticles (MNPs) can be used to enhanced photodetector performance and this same technique is now commonly applied in research to enhance thin-film solar cells.[13,14]

The location of the MNPs is an important consideration when trying to maximize the solar cell efficiency. While front located MNPs may have the potential to be an effective anti-reflection coating, they cause a reduction in absorption below the MNP resonance due to the interference of incident and scattered light, which is known as the Fano effect.[15,16] Placing MNPs at the rear of the cell avoids the Fano loss mechanism. Rear located MNPs should be kept close to the substrate to maximize the coupling of light into the substrate[17,18] and the MNPs should be relatively short, or flat, to keep the plasmon mode close to the substrate.[19] Experiments using mono- and multi-crystalline silicon solar cells have shown that the current density (J_{sc}) can be enhanced by adding MNPs to the rear of the cell[16,20,21] and can be further enhanced by adding a supporting reflector behind the MNPs.[22–30] Rear located MNPs with a rear reflector have also been shown to enhance the performance of various thin-film silicon solar cells.[31–43]

Whereas MNPs have been shown to have a positive impact on the performance of thin-film silicon solar cells, optimizing the design of the MNP with reflector support, which will be referred to as a plasmonic back reflector (PBR), is often overlooked. The size of the NPs and distance to the active layer have been the focus in many studies. The distance between the NPs and the mirror also has a significant impact on the scattering properties of the PBR. This distance can be adjusted to tune the MNP response[44] and modify the diffuse scattering properties.[45,46] Analyzing the PBR without the solar cell can provide comparison to standard textured substrates by calculating the reflection and haze of the substrates, but Santebergen et al. has shown that the response of a PBR can change drastically when the layers of the solar cell are added to the structure.[47] Tan *et al.* has provided an experimental analysis that shows how the PBR design can affect the performance of an a-Si:H solar cell, considering both the optical and electrical performance.[33] However, they used a substrate design leading to changes in performance that may have been caused by roughness of the MNP layer. In this paper, we investigate the design of a PBR for a superstrate a-Si:H solar cell. The main parameters investigated are the size of the MNPs, the distance between the MNPs and the a-Si:H, and the distance between the MNPs and the rear reflector. We also fabricated devices that match the optimal designs found in the simulations.

PLASMONIC BACK REFLECTOR DESIGN

Simulations of the PBR were done to guide experimental work. Lumerical FDTD[48] was used for the simulations. The goal was to design a PBR to enhance the absorption in the active layer of an a-Si:H solar cell. A standard superstrate a-Si:H structure, which consist of a glass substrate coated with Fluorinated Tin Oxide (FTO). The thickness of the a-Si:H layer influences the PBR design, but to reduce the number of parameters being investigated, the active layer thickness was fixed at 300 nm. Four design parameters were varied: the TCO spacer thickness between the a-Si:H and the MNPs (d_{top}), the radius of the hemispherical MNPs (d_{rad}), the TCO spacer between the NPs and the metallic mirror (d_{bot}), and the type of TCO. The TCO coating the MNP, d_{bot}, was assumed to be conformal, which results in the metallic mirror being curved. This was done for two reasons. First, this more closely represents an experimental device. Second, this allows for the mirror to MNP spacing to be constant at all points along the MNP surface. Fig. 1 shows a sketch of the simulated design. Simulations were done in 3D and to reduce the simulation run times, periodic boundary conditions were used in the x and y directions. Perfectly Matched Layers (PML) were used in the z direction. The period of the MNP array was fixed at $4\times d_{rad}$. The software's built in conformal meshing algorithm was used except over the MNP and the curved part of the mirror, which had a 1nm mesh override region to increase simulation accuracy. The MNP and metallic mirror were both set as Ag for the simulations. To further reduce simulation times, the simulations were run for wavelengths

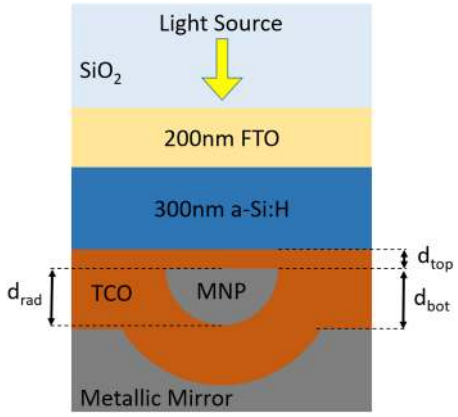

FIG. 1. Schematic of the simulated device. This layout was chosen to match a possibly fabrication process. The MNP could be deposited onto a TCO spacer, d_{top}, and a conformal layer of the same TCO could be deposited over the MNP, d_{bot}. The assumption of a conformal coating transfers the pattern into the metallic mirror.

from 500 nm to 800 nm. This is because wavelengths below 500nm are absorbed, or reflected, before they can interact with the rear reflector. The n&k values for a-Si:H were obtained by using ellipsometry of films deposited by Plasma-Enhanced Chemical Vapor Deposition (PECVD) at our facility. The values for FTO were obtained in Ref. 49 and Aluminum-doped Zinc Oxide (AZO) were obtained from Ref. 50. SiO_2 values were fitted using data from Palik[51] and Ag values were fitted using data from Johnson and Christy.[52]

Fig. 2 shows the results from simulations utilizing AZO as the TCO layer in the PBR design. Only two values of the d_{top} were tested; 0 nm and 10 nm. We selected these values because the ideal location for rear located NPs is to be as close to the active layer as possible to improve light coupling.[16] While the 0 nm spacer layer is expected to perform better than a design using a spacer, the spacer layer may be necessary to prevent the NPs from being in direct contact with the a-Si:H. Ag in contact with a-Si:H may lead to increased carrier recombination, potentially reducing or eliminating any improvement in optical performance. The NP radius was varied by 5 nm steps from 30 nm to 85 nm and the bottom TCO was varied by 10nm steps from 10 nm to 100 nm. The design with a 0 nm TCO top layer shows the greatest enhancement, reaching a 7.2% increase in absorption over the 500-800nm wavelength range with a bottom TCO of 60 nm and a NP radius of 75 nm. The reason for this increase can be seen in Fig. 3. The PBR leads to an increase in the absorption of the near bandgap light. Fig. 2 also shows enhancement greater than 5% can be achieved with NP radius ranging from 60 nm to 80 nm and a bottom TCO thickness ranging from 50 nm to 80 nm, indicating that the experimental device may have wide fabrication tolerances.

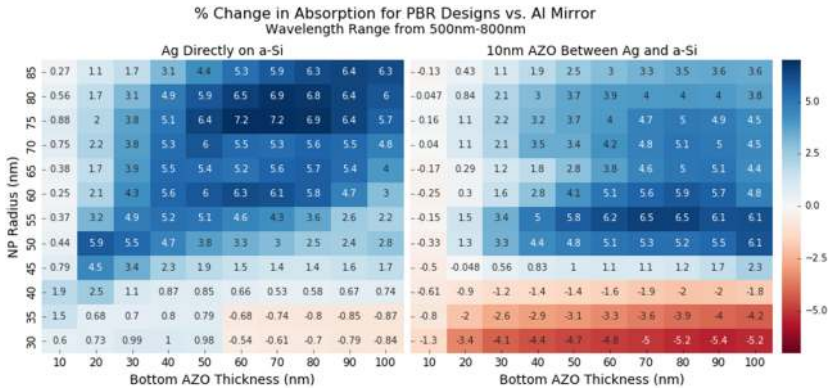

FIG. 2. Change in a-Si:H absorption for various PBR design using AZO.

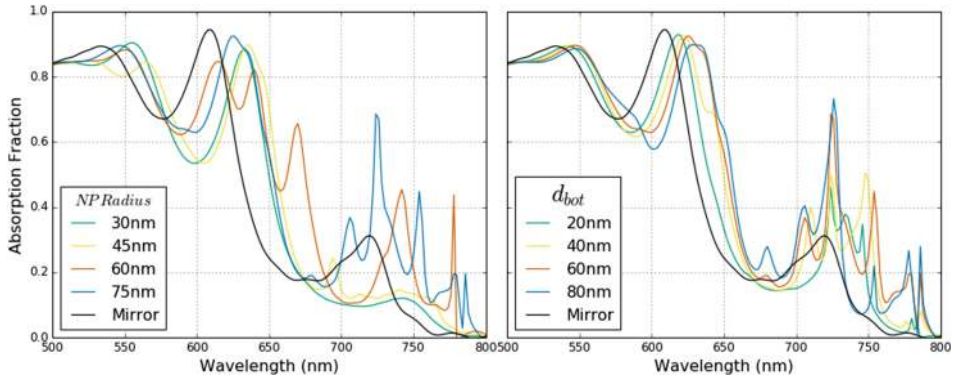

FIG. 3. Plots showing how absorption versus wavelength changes with the MNP radius and bottom AZO thickness. The black line indicates absorption in 300 nm a-Si:H that only uses a metallic mirror. The plot on the left shows how absorption changes as the NP radius is increased and with a constant bottom AZO thickness of 60 nm. The plot on the right shows how absorption changes as the bottom AZO thickness is increased, with a constant NP radius of 75 nm. Both plots show data for MNPs in direct contact with the a-Si:H (i.e. no spacer).

As mentioned, an important concern about the simulated design is the effect of having MNPs in direct contact with the a-Si:H. While these simulations provide insight into the optical performance of a solar cell, they neglect the electrical performance. A spacer layer between the MNPs and the a-Si:H may be necessary to optimize both the electrical and optical performance.[33] Fig. 2 also shows the results of the design with a 10 nm spacer between the a-Si:H and MNP. This spacer has a large effect on the optical performance. The peak enhancement is reduced to 6.51% with a NP radius of 55 nm and a bottom TCO of 80 nm. Also, the negative effect of smaller MNPs becomes more prominent. This is important to consider when fabricating experimental devices with MNPs. The negative impact of smaller MNPs may outweigh the positive effect of the larger MNPs if the size distribution of the particles are large.

In PBRs, and most rear located MNP designs, large field concentrations between the mirror and MNP can lead to losses if the material in that region has non-negligible absorption. The n&k values used in this paper for AZO may lead to increased efficiency, but the properties of AZO can vary and there are other options for TCO's. Solar cells require a low absorbing, but high conductivity TCO for optimal performance. Another commonly used TCO for solar cells is Indium Tin Oxide (ITO), which has a higher conductivity then AZO. Absorption is also higher in ITO. Fig. 4 shows how device performance can change when using ITO as the TCO material. The ITO n&k values were fitted to data from the Sopra database.[53] While the location of peak enhancement has only slightly changed, the maximum enhancement is reduced.

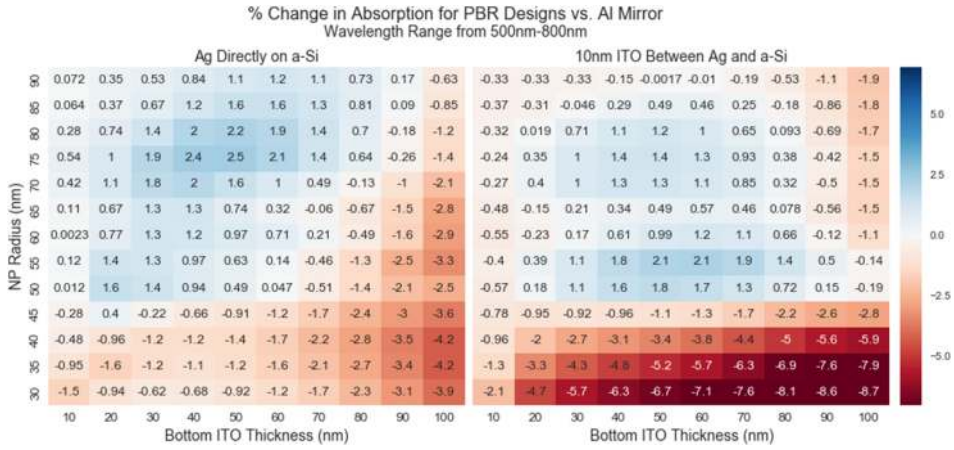

FIG. 4. Change in a-Si:H absorption for various PBR design using ITO.

MATERIALS AND METHODS

Solar cells were fabricated in the superstrate configuration. 1"x1" FTO coated glass (TEC15) was acquired from MTI Corporation and cleaned with detergent and acetone, followed by a one-hour Ultra-Violet Ozone (UVO) clean to remove any contaminant molecules prior to deposition. A (pin)a-Si:H solar cell was deposited on the FTO glass using a single chamber PECVD; the Trion Technologies Orion II PECVD. The dopant gases were TMB and phosphine. Depositions were done at 200°C. The p-layer was 12nm thick, i-layer was 300 nm thick, and the n-layer was 25 nm thick. The thicknesses were estimated from the deposition rate of each layer measured from test samples with a Veeco Dektak 150 profilometer. Baseline solar cells (i.e. controls) were fabricated by adding a 150 nm aluminum mirror to the back of the cells. This is a known discrepancy from the simulations. Experiments revealed that our process was more stable with Al versus Ag. Ag resulted in significant degradation of the baseline solar cells and skewed the analysis. Therefore, Al was used for the experiments in this work. The Al was thermally evaporated using a tungsten "Z" coil from R.D. Mathis Company in an Angstrom Engineering Amod deposition system. Four cells were fabricated on each 1"x1" sample by using a thin, stainless steel shadow mask with four 5 mm diameter holes during the aluminum deposition. The solar cell parameters for the best cell from a control cell and a cell with 50 nm ITO spacer before the Al mirror are shown in Table I.

The PBR was fabricated by adding TCO and Ag films prior to the Al mirror deposition. These cells were masked using the same shadow mask mentioned above during TCO and Ag depositions to avoid any shorting at the edges of the sample. TCOs were deposited using RF sputtering in an Angstrom Engineering Amod tool. While simulations showed that AZO should be an option, the AZO deposited using available tools has yet to achieve resistivity values low enough to use in a solar cell application. Therefore, ITO was deposited from a 2" target acquired from Angstrom Engineering. The RF power was set to 100 W, chamber pressure set to 2 mT, and flow rates of 20 sccm Ar and 0.2 sccm O_2 were used. Thickness was estimated by determining the deposition rate by measuring the thickness of a test sample using a profilometer prior to fabricating any PBR enhanced devices. A device with a 50 nm ITO layer and a 150 nm Al mirror was fabricated to verify that the ITO did not significantly alter the performance of the reference solar cell. The solar cell parameters are shown in Table I.

The MNPs were fabricated by using thermal dewetting. Thin-films of Ag were thermally evaporated from a Molybdenum boat source from R.D. Mathis Company at a rate of 1 Å/s. The mass thickness of the film was estimated by depositing a 50 nm Ag film under the same conditions onto Corning Eagle XG glass. This film was measured with the profilometer and this measurement was used to set the tooling factor for the following depositions. After the Ag films were deposited, the samples were placed in a MTI OTF-1200X Tube Furnace. Annealing was done in a forming gas of Ar and H2, with flow rates of 100 sccm and 10 sccm respectively. Samples were annealed at 200°C for 60 minutes. SEM micrographs of an 8nm film deposited directly on the a-Si:H, using a TEC15 substrate, before and after annealing are shown in Fig. 5.

Several factors can be adjusted to modify the resulting nanoparticles morphology; two main factors are the substrate and Ag film thickness. For this work, there were two substrates of interest: a-Si:H and ITO. A small set of samples was fabricated for MNP analysis. The SEM micrographs were analyzed using ImageJ.[54] Results of the analysis are shown in Fig. 6. Increasing the Ag mass thickness increases the MNP diameter. Increasing the Ag mass thickness reduces the circularity of the MNPs. MNPs formed directly on a-Si:H have a narrower distribution than the MNPs formed on the ITO spacer layer. These effects have been documented earlier.[12,55–58] This process leads to a relatively broad distribution of MNP diameters. As was mentioned with the simulation results,

TABLE I. Results for a control cell and a cell with 50nm ITO deposited before the Al mirror.

Sample	J_{sc} (mA/cm^2)	V_{oc} (V)	Efficiency (%)	Fill Factor
Control	11.14	0.82	4.99	0.55
50nm ITO	11.51	0.82	4.99	0.53

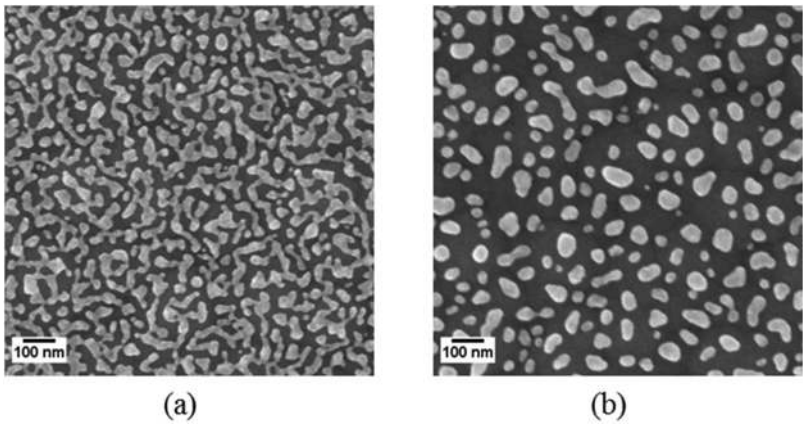

FIG. 5. An 8nm mass thickness Ag film deposited on TEC15 FTO glass (a) as deposited, and (b) after annealing.

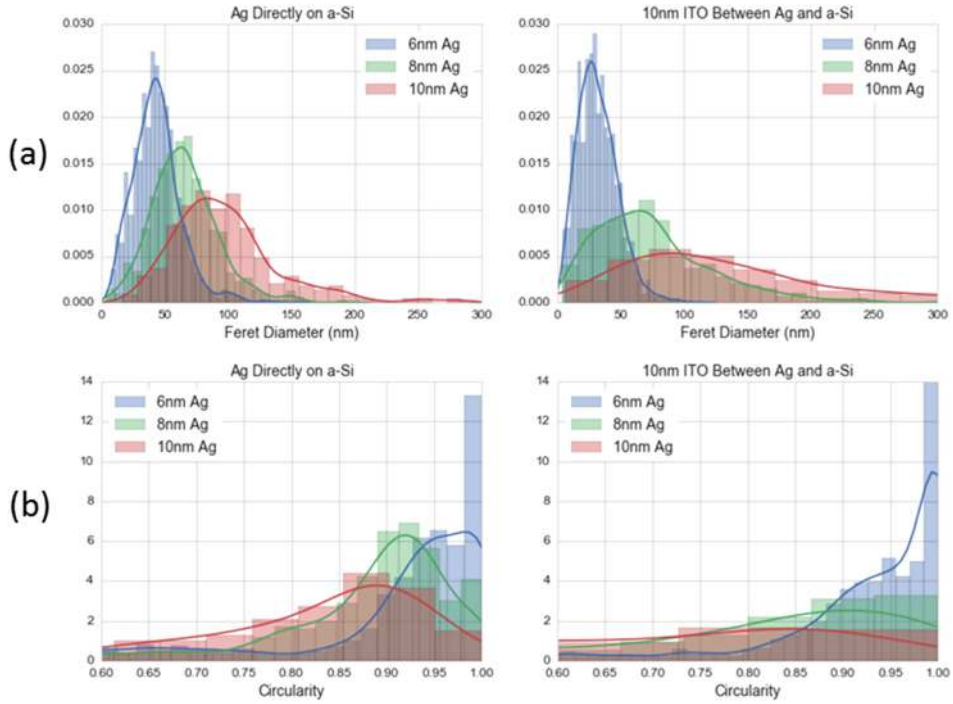

FIG. 6. Histograms of the MNPs (a) feret diameter and (b) circularity, with kernel density estimates shown for each dataset. The legends correspond to the mass thickness of the deposited films.

the fabrication tolerances for the solar cell design is relatively broad, but the smaller MNPs have a negative impact on the potential enhancement. Also, the thicker Ag films create larger MNPs, but these films still suffer from the negative impact of the smaller MNPs. While this fabrication process is simple and can be easily applied to large areas, a process with more control over the MNP size is likely required to eliminate losses due to small MNPs.

A significant difference between the simulated design and the experimental design was the front FTO. In the simulations, the front FTO was flat and in the experiments the front FTO was textured. This results in scattering of the incident light at the front of the cell and likely affected how the MNPs respond. More importantly, the textured surface played a large role in the MNP fabrication process. Fig. 7(a) shows an Ag film annealed on a (pin)a-Si:H solar cell deposited on TEC7 glass. The image shows a valley where the MNPs are clearly smaller than the MNPs on the peaks. This likely results from the directionality of the Ag thermal evaporation. The peaks shadow the valleys, resulting in film

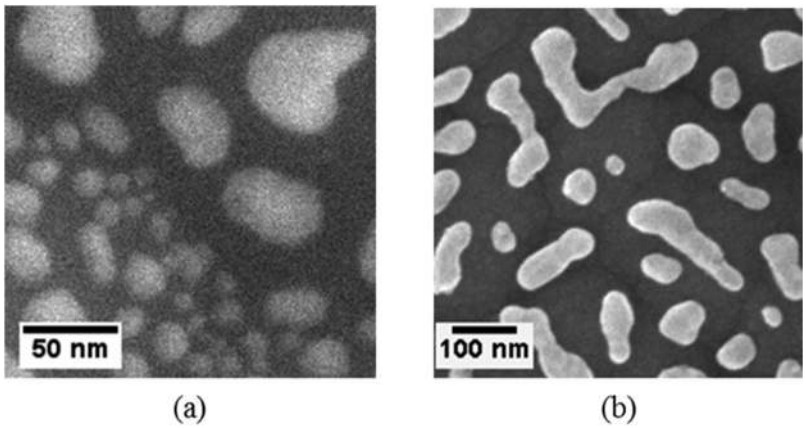

FIG. 7. (a) SEM micrograph of an annealed 10 nm Ag film on a solar cell using a TEC7 substrate, showing the variation in MNP size at a relatively sharp feature. (b) A lower magnification SEM micrograph of a 10 nm film on a solar cell using a TEC15 substrate. Note that the issue with the valleys has been mostly eliminated by switching substrates. The problem was not eliminated, but the effect had been reduced.

thickness variations between the peaks and valleys. This would have a detrimental effect on the solar cell performance, as shown by the simulations. The substrate was switched to TEC15 due to its lower haze value, reducing the shadowing effect of the high haze TEC7 glass. An annealed 10 nm Ag film on a solar cell deposited on TEC15 glass is shown in Fig. 7(b).

After the MNPs were fabricated, cells were moved to the Angstrom sputter system for the bottom ITO layer, and then completed in the thermal evaporator for the Al mirror. The solar cells were characterized by illuminated Current-Voltage (IV) sweeps and External Quantum Efficiency (EQE). The IV sweeps were taken under 1 sun illumination using a Xenon lamp with a AM1.5g filter. The lamp power was calibrated by using a 6mm diameter mask over a reference cell with a KG5 window from ABET Technologies. The IV curves were used to calculate the overall efficiency, short circuit current (J_{sc}), open circuit voltage (V_{oc}), and the fill factor (FF). EQE measurements were taken using a Fianum supercontinuum laser with a Thorlabs PM100D power meter.

RESULTS AND DISCUSSION

Experimental devices were fabricated to determine if the presented design may lead to enhancement in the J_{sc} and overall efficiency. All solar cells were fabricated on the TEC15 FTO glass with a 300 nm thick i-layer. Fig. 8 shows the solar cell parameters and IV curves of the best cells for each device for various Ag film mass thicknesses.

The data shows that as the film thickness decreases, which corresponds to a decrease in MNP size, the performance of the solar cell degrades. The 10 nm film was the best performing device with the PBR design, but this device was still worse than the control sample. These results correlate with the simulation data. In the previous section the 10 nm film was shown to have a MNP size distribution located around a diameter of about 100 nm. This is below the ideal MNP size of about 150 nm diameter shown in Fig. 4. While the simulation data does show that a MNP of 100 nm diameter and a 50 nm bottom ITO layer should slightly outperform the control, the large distribution in the MNP size lead to an overall decrease in performance. A maximum thickness of 10 nm for the Ag film was chosen because thicker films formed less uniform MNPs. Even though the peak of the MNP diameter distribution could be shifted towards the goal of 150 nm diameter MNPs, the large variation in MNP size and shape at and above 12 nm Ag mass thickness would have an unknown effect.

The fabrication process does suffer from variability between each sample set. To verify that the above results are correct two more experiments were run with the goal of increasing the size of the dataset. Eight devices were fabricated during a single run of the PECVD. Four devices were controls and four devices had a PBR. Each device had four test points, leading to 16 data points

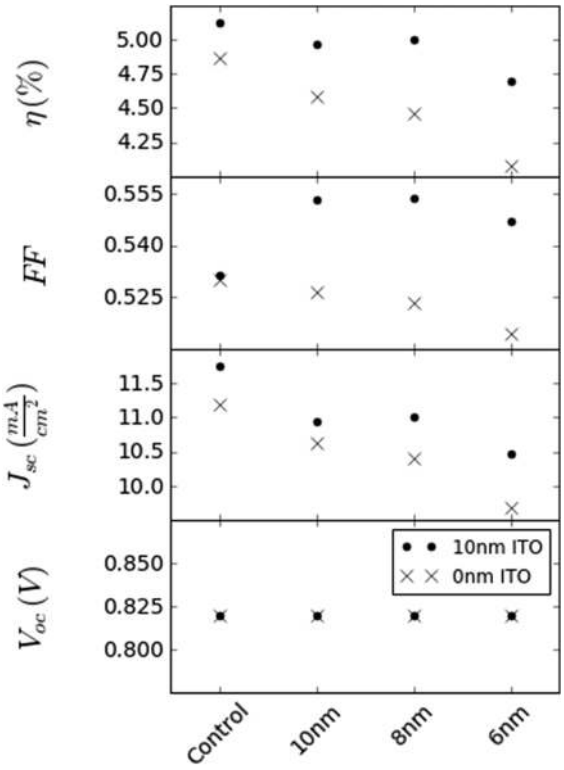

FIG. 8. The solar cell parameters of the PBR based devices with a control. The thicknesses correspond to the mass thickness of the deposited Ag film. One device was fabricated for each Ag thickness, and each device consisted of four cells. The best cell for each device is plotted here. The black dots show the best cell for a 10 nm ITO spacer and the black crosses show the best cell for a 0 nm ITO spacer.

for each device set. The first experiment placed the MNPs directly on the a-Si:H (i.e. no ITO spacer), and the second experiment used a 10 nm ITO spacer. The results of these experiments are shown in Fig. 9. These two experiments confirmed that the MNP devices performed slightly worse than the control devices. The EQE of the best device from each device set is shown in Fig. 10. The EQE results show that the controls and MNP devices had similar responses below about 550 nm, which agrees with the simulations. Wavelengths below 550 nm are reflected or absorbed before interacting with the back reflector. Above 550 nm there are small discrepancies between the controls and their respective MNP cells. While there are a few areas that the MNP cells have a higher EQE, these slight advantages do not compensate for the additional losses.

There are three main reasons that explain why the experimental devices did not achieve the performance enhancement predicted by simulation. (1) the TCO used was ITO, which has a higher absorption coefficient than AZO. (2) the MNPs fabricated were too small. (3) the size distribution of the MNPs was large. The first problem could be corrected by just switching to AZO. The second and third problems are related to the dewetting process for the formation of the MNPs. A different approach towards MNPs fabrication may be required to eliminate these problems. Switching to a substrate configuration may prove beneficial. In this configuration, the PBR can be fabricated prior to depositing the a-Si:H, which allows for dewetting at higher annealing temperatures. Another option would be to spin or spray coat on pre-fabricated colloidal Ag MNPs. Colloidal MNPs can be made to the desired size with narrow distributions.

Another discrepancy between the experimental and simulated devices is the surface coverage and periodicity of the MNPs. The simulations were run with a simulation width of only four times the NP radius, which leads to a high MNP surface coverage of 50%. This was done to reduce the computational time required for each simulation. The surface coverage of the experiment devices was about 30-40%, as shown in Fig. 11(a). A set of simulations using AZO and a NP with a 50 nm radius was run with a simulation width of six times the MNP radius. Fig. 11(b) shows that increasing

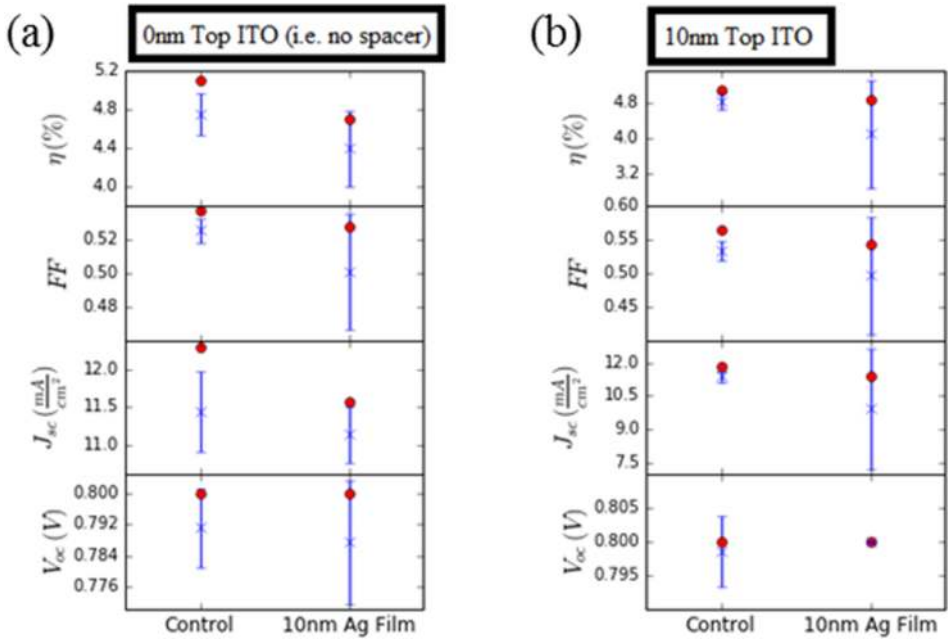

FIG. 9. Solar cell parameters for (a) MNPs directly on the a-Si:H, and (b) a 10 nm ITO spacer between the a-Si:H and the MNPs. A 10 nm mass thickness Ag film was used for these devices.

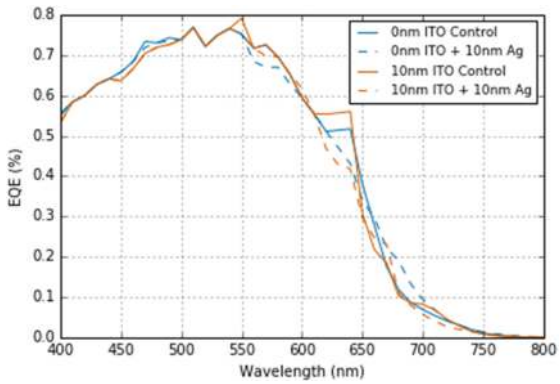

FIG. 10. EQE of the best control samples and the best MNP samples using a 10nm mass thickness Ag film. These plots correspond to the IV curves shown in Fig. 9.

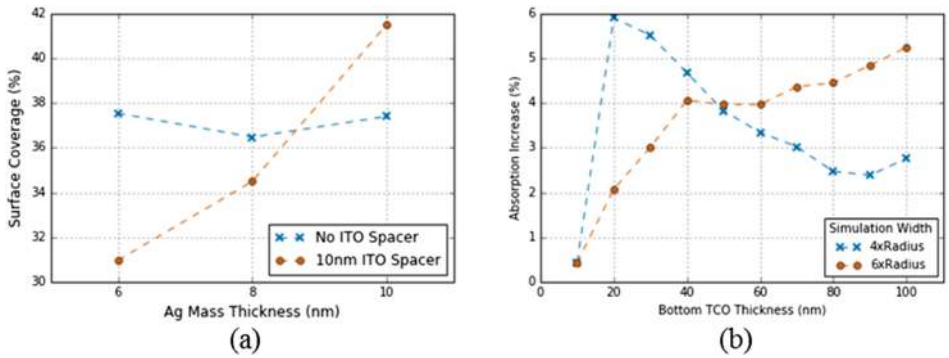

FIG. 11. (a) Surface coverage of a MNP film versus the deposited Ag mass thickness. (b) Simulated absorption of a device with a 50nm radius Ag NP versus bottom TCO thickness, which was AZO in this case, at two different simulation widths. 4xRadius represents a 50% coverage and 6xRadius is a 33.3% coverage.

the simulation width shifted peak enhancement to a thicker bottom TCO. This does indicate that the experimental devices may have performed better with a thicker bottom TCO layer. While this may not be the case at every NP radius, it can be a factor in the performance decrease found in our experimental devices. Also, the simulations were run with periodic boundary conditions. This means that the simulated device was a 2D array of MNPs instead of the random distribution that was fabricated. Akimov and Koh have shown in simulations that enhancement due to front side MNP gratings are quite stable with respect to MNP position deviations, but large position deviations can significantly reduce the desired performance enhancement.[59]

CONCLUSION

Simulations of a 300 nm solar cell with a PBR were shown to increase the absorption in the a-Si:H. The simulations also show that when adding MNPs to the back reflector of a solar cell it is important to consider the distances between each of the device's layers. Ag MNPs with a diameter of 150 nm directly on the a-Si:H and a 60 nm AZO layer between the MNPs and the mirror lead to a maximum absorption increase of 7.2% in the 500 nm to 800 nm wavelength range. Due to the structure of a PBR, there are large fields within the TCO. The absorption of the TCO can significantly reduce the light trapping effects of a PBR. The experimental devices did not demonstrate enhancement. This is likely due to the use of ITO instead of AZO, and the MNPs being too small with a large distribution in size. Overcoming these issues is possible. AZO is a commonly used TCO, but ITO was chosen due to current limitations in our facility. Controlling the MNPs size is more difficult and switching to a colloidal NP process may be required. Improving the performance of a solar cell, such as the one used in this study, with a PBR should be possible, but the benefits may not outweigh the increased complexity in fabrication. Also, while MNPs are good scatterers, the simulations did not compare how well the MNPs performed against a common, textured device. A textured device may be able to benefit from the MNPs due to their ability to strongly influence the back reflectors response in the near band-gap energies for a-Si:H.

[1] A. Luque and S. Hegedus, *Handbook of photovoltaic science and engineering*, 2nd ed. (Wiley, 2011).
[2] X. Deng and E. A. Schiff, in *Handbook of Photovoltaic Science and Engineering* (John Wiley & Sons, Ltd, 2003), p. 505.
[3] K. L. Chopra, P. D. Paulson, and V. Dutta, Progress in Photovoltaics **12**, 69 (2004).
[4] E. Yablonovitch, Journal of the Optical Society of America **72**, 899 (1982).
[5] J. Müller, B. Rech, J. Springer, and M. Vanecek, Solar Energy **77**, 917 (2004).
[6] C. Battaglia, M. Boccard, F.-J. Haug, and C. Ballif, Journal of Applied Physics **112**, 094504 (2012).
[7] S. Hiroshi, Y. Takasi, H. Toshio, and I. Yukimi, Japanese Journal of Applied Physics **29**, 630 (1990).
[8] H. B. T. Li, R. H. Franken, J. K. Rath, and R. E. I. Schropp, Solar Energy Materials and Solar Cells **93**, 338 (2009).
[9] M. G. Deceglie, V. E. Ferry, A. P. Alivisatos, and H. A. Atwater, IEEE Journal of Photovoltaics **3**, 599 (2013).
[10] Z. Yu, A. Raman, and S. Fan, Applied Physics A **105**, 329 (2011).
[11] H. R. Stuart and D. G. Hall, Applied Physics Letters **69**, 2327 (1996).
[12] H. R. Stuart and D. G. Hall, Applied Physics Letters **73**, 3815 (1998).
[13] H. A. Atwater and A. Polman, Nature Materials **9**, 205 (2010).
[14] M. Gu, Z. Ouyang, B. Jia, N. Stokes, X. Chen, N. Fahim, X. Li, J. Ventura Michael, and Z. Shi, Nanophotonics **1**, 235 (2012).
[15] P. Spinelli, M. Hebbink, R. de Waele, L. Black, F. Lenzmann, and A. Polman, Nano Lett **11**, 1760 (2011).
[16] F. J. Beck, S. Mokkapati, A. Polman, and K. R. Catchpole, Applied Physics Letters **96**, 033113 (2010).
[17] F. J. Beck, S. Mokkapati, and K. R. Catchpole, Optics Express **19**, 25230 (2011).
[18] F. J. Beck, E. Verhagen, S. Mokkapati, A. Polman, and K. R. Catchpole, Optics Express **19**, A146 (2011).
[19] S. Mokkapati, F. J. Beck, R. de Waele, A. Polman, and K. R. Catchpole, Journal of Physics D: Applied Physics **44**, 185101 (2011).
[20] F. J. Beck, A. Polman, and K. R. Catchpole, Journal of Applied Physics **105**, 114310 (2009).
[21] S. Pillai, F. J. Beck, K. R. Catchpole, Z. Ouyang, and M. A. Green, Journal of Applied Physics **109**, 073105 (2011).
[22] A. Basch, F. J. Beck, T. Söderström, S. Varlamov, and K. R. Catchpole, Applied Physics Letters **100**, 243903 (2012).
[23] F. J. Beck, S. Mokkapati, and K. R. Catchpole, Progress in Photovoltaics: Research and Applications **18**, 500 (2010).
[24] Z. Ouyang, S. Pillai, F. Beck, O. Kunz, S. Varlamov, K. R. Catchpole, P. Campbell, and M. A. Green, Applied Physics Letters **96**, 261109 (2010).
[25] Z. Ouyang, X. Zhao, S. Varlamov, Y. Tao, J. Wong, and S. Pillai, Progress in Photovoltaics: Research and Applications **19**, 917 (2011).
[26] J. Park, N. Park, and S. Varlamov, Applied Physics Letters **104**, 033903 (2014).
[27] J. Rao, S. Varlamov, J. Park, S. Dligatch, and A. Chtanov, Plasmonics **8**, 785 (2012).
[28] S. Varlamov, J. Rao, and T. Soderstrom, Journal of Visualized Experiments 4092 (2012).

[29] Y. Yang, S. Pillai, H. Mehrvarz, H. Kampwerth, A. Ho-Baillie, and M. A. Green, Solar Energy Materials and Solar Cells **101**, 217 (2012).
[30] Y. Zhang, B. Jia, Z. Ouyang, and M. Gu, Journal of Applied Physics **116**, 124303 (2014).
[31] X. Chen, B. Jia, J. K. Saha, B. Cai, N. Stokes, Q. Qiao, Y. Wang, Z. Shi, and M. Gu, Nano Lett **12**, 2187 (2012).
[32] C. Eminian, F. J. Haug, O. Cubero, X. Niquille, and C. Ballif, Progress in Photovoltaics: Research and Applications **19**, 260 (2011).
[33] H. Tan, R. Santbergen, G. Yang, A. H. M. Smets, and M. Zeman, IEEE Journal of Photovoltaics **3**, 53 (2013).
[34] M. Hidenori, S. Hitoshi, M. Koji, T. Hidetaka, and K. Michio, Applied Physics Express **7**, 112302 (2014).
[35] M. Hidenori, S. Hitoshi, M. Koji, and K. Michio, Japanese Journal of Applied Physics **51**, 042302 (2012).
[36] E. Moulin, P. Luo, B. Pieters, J. Sukmanowski, J. Kirchhoff, W. Reetz, T. Müller, R. Carius, F.-X. Royer, and H. Stiebig, Applied Physics Letters **95**, 033505 (2009).
[37] E. Moulin, J. Sukmanowski, P. Luo, R. Carius, F. X. Royer, and H. Stiebig, Journal of Non-Crystalline Solids **354**, 2488 (2008).
[38] E. Moulin, J. Sukmanowski, M. Schulte, A. Gordijn, F. X. Royer, and H. Stiebig, Thin Solid Films **516**, 6813 (2008).
[39] R. Santbergen, R. Liang, and M. Zeman, in *A-Si:H solar cells with embedded silver nanoparticles*, 2010 (IEEE), p. 000748.
[40] H. Tan, R. Santbergen, A. H. Smets, and M. Zeman, Nano Lett **12**, 4070 (2012).
[41] H. Tan, L. Sivec, B. Yan, R. Santbergen, M. Zeman, and A. H. M. Smets, Applied Physics Letters **102**, 153902 (2013).
[42] J. D. Winans, C. Hungerford, K. Shome, L. J. Rothberg, and P. M. Fauchet, Optics Express **23**, A92 (2015).
[43] S. Morawiec, M. J. Mendes, S. A. Filonovich, T. Mateus, S. Mirabella, H. Águas, I. Ferreira, F. Simone, E. Fortunato, R. Martins, F. Priolo, and I. Crupi, Optics Express **22**, A1059 (2014).
[44] W. R. Holland and D. G. Hall, Physical Review Letters **52**, 1041 (1984).
[45] M. J. Mendes, S. Morawiec, F. Simone, F. Priolo, and I. Crupi, Nanoscale **6**, 4796 (2014).
[46] R. S. A. Sesuraj, T. L. Temple, and D. M. Bagnall, Solar Energy Materials and Solar Cells **111**, 23 (2013).
[47] R. Santbergen, H. Tan, M. Zeman, and A. H. Smets, Optics Express **22**, A1023 (2014).
[48] https://www.lumerical.com/.
[49] J. Chen, PhD diss. Thesis, University of Toledo, 2010.
[50] AZO Transparent Conductive Coating, http://materion.com/ResourceCenter/ProductData/InorganicChemicals/Oxides/AZOTransparentConductiveCoating.aspx (Jan. 28, 2015).
[51] E. D. Palik, *Handbook of Optical Constants of Solids* (Elsevier Science, 2012).
[52] P. B. Johnson and R. W. Christy, Physical Review B **6**, 4370 (1972).
[53] Optical Data from Sopra SA, http://www.sspectra.com/sopra.html (Nov. 10, 2014).
[54] W. Rasband, *U.S. National Institutes of Health*, Bethesda, Maryland, USA, http://rsb.info.nih.gov/ij/, (1997-2015).
[55] M. C. Gunendi, I. Tanyeli, G. B. Akguc, A. Bek, R. Turan, and O. Gulseren, Optics Express **21**, 18344 (2013).
[56] I. Tanyeli, H. Nasser, F. Es, A. Bek, and R. Turan, Optics Express **21**, A798 (2013).
[57] J. P. Clarkson, PhD diss. Thesis, University of Rochester, 2010.
[58] J. D. Winans, Dissertation Thesis, University of Rochester, 2013.
[59] Y. A. Akimov and W. S. Koh, Applied Physics Letters **99**, 063102 (2011).